Heliyon

ELSEVIER

Received:
4 November 2015
Revised:
10 October 2016
Accepted:
24 November 2016

Heliyon 2 (2016) e00209

The effect of absorbed hydrogen on the dissolution of steel

Sebastian Thomas [a,*], **Noemie Ott** [a,b], **Rebecca F. Schaller** [a,c], **Jodie A. Yuwono** [a], **Polina Volovitch** [b], **Guruprasad Sundararajan** [d], **Nikhil V. Medhekar** [a], **Kevin Ogle** [b], **John R. Scully** [c], **Nick Birbilis** [a]

[a] *Department of Materials Science and Engineering, Monash University, Clayton, Victoria 3800, Australia*

[b] *Chimie ParisTech, Ecole Nationale Supurieure de Chimie de Paris, Paris 75005, France*

[c] *Department of Materials Science and Engineering, University of Virginia, Charlottesville, VA 22904, USA*

[d] *GE Global Research, Bangalore 560066, India*

* Corresponding author.

E-mail address: Sebastian.Thomas@monash.edu (S. Thomas).

Abstract

Atomic hydrogen (H) was introduced into steel (AISI 1018 mild steel) by controlled cathodic pre-charging. The resultant steel sample, comprising about 1 ppmw diffusible H, and a reference uncharged sample, were studied using atomic emission spectroelectrochemistry (AESEC). AESEC involved potentiodynamic polarisation in a flowing non-passivating electrolyte (0.6 M NaCl, pH 1.95) with real time reconciliation of metal dissolution using on-line inductively coupled plasma-atomic emission spectroscopy (ICP-OES). The presence of absorbed H was shown to significantly increase anodic Fe dissolution, as evidenced by the enhanced detection of Fe^{2+} ions by ICP-OES. We discuss this important finding in the context of previously proposed mechanisms for H-effects on the corrosion of steels.

Keywords: Engineering, Materials Science

1. Introduction

Steels come in regular contact with hydrogen-bearing and/or producing environments. This may occur during the transportation or storage of hydrogen (H), or as a

http://dx.doi.org/10.1016/j.heliyon.2016.e00209

result of corrosion of steel in a low pH environment (an example being the hydrogen sulphide based sour environment), corrosion in poorly aerated environments, overprotection from cathodic protection, or in atmospheric exposure to marine aerosols [1, 2, 3, 4, 5, 6, 7, 8, 9, 10, 11, 12, 13]. In such cases, hydrogen evolution from the reduction of water is the main cathodic reaction taking place on the steel surface. Even the localised or pitting corrosion of stainless steels is accompanied by hydrogen evolution [13]. Several elementary reaction steps take place upon a metal surface during the hydrogen evolution reaction, including hydrogen adsorption, recombination and importantly absorption of atomic hydrogen into metal [14, 15].

Hydrogen in steel (and many metals) is historically known to lead to hydrogen embrittlement (HE), and also contributes to a ductile to brittle transition of steel [16, 17, 18, 19]. However, the exact mechanism by which hydrogen embrittles steel is a topic of some debate, as summarised very recently by Robertson et al. [18]. The fact that hydrogen cannot be 'seen' by methods such as electron microscopy, and its time dependent existence and mobility frustrates other analytical methods which are necessarily cumbersome (for example if trying to isolate a crack tip) has therefore led to a number of theories for hydrogen embrittlement. The prominent mechanisms of hydrogen embrittlement include the hydrogen enhanced decohesion mechanism (HEDE), adsorption induced dislocation emission (AIDE), hydrogen enhanced localised plasticity (HELP), or hydride (i.e. brittle hydride) formation, in addition to many other less conventional theories. A detailed description of such mechanisms is available elsewhere [16, 17, 18, 19, 20, 21, 22, 23]. Such mechanisms however propose a purely mechanical/metallurgical framework, which rationalises the hydrogen assisted cracking of steel, under some applied stress.

However, somewhat surprisingly, the effect of hydrogen or dissolved hydrogen in steel with respect to the unit processes in anodic dissolution, or cathodic reduction, that govern its chemical and electrochemical behaviour is not well clarified (in the condition of zero applied stress, or even under stress). If one considers HE as a form of stress corrosion cracking, then the 'corrosion' component is clearly an important factor, albeit that it is not integrated into any models of embrittlement. To date, works that deal with environmentally assisted cracking (which is a term that encompasses both hydrogen embrittlement and stress corrosion cracking) do not assume H to be an independent electrochemical or a chemical entity within steel. Further, most electrochemistry texts will not have a definitive statement on the role of hydrogen; for example, how does absorbed hydrogen impact the electrode potential? Does it increase rates of reaction? Does it have no effect? These seemingly simple questions are what the present work seeks to answer.

It is known that atomic hydrogen within metals can serve as a strong reducing agent [24], recently it was found to reduce several metals including as Cu, Sb, Sn,

http://dx.doi.org/10.1016/j.heliyon.2016.e00209

Bi etc., from their salt solutions. The reduction potential for H/H^+ from those studies was found to be in the range −0.17 to −0.24 V_{SHE}, in the pH range 3 to 4. Schaller et al. [25] demonstrated using SECM that hydrogen charged steel surfaces consumed (reduced) more oxygen when compared to uncharged steel surfaces. It was proposed that diffusible atomic hydrogen (H_{Diff}) may directly reduce oxygen in solution, by a fuel-cell like reaction [25].

Several researchers have shown that the kinetics of steel dissolution (as measured electrochemically) is apparently increased in hydrogen charged steels [26, 27, 28, 29, 30, 31, 32, 33, 34, 35, 36, 37, 38, 39]. The presence of H also has been found to increase the corrosion of other systems, including pure Cr and Ni-Cr based systems [40, 41, 42]. Li et al. [28] showed that for the X-70 steel, hydrogen charging enhanced the electrochemically determined anodic kinetics by a factor of about ~50% (at a potential of −0.4 V_{SCE}). They attributed this phenomenon to the alteration in the chemical potential and the exchange current density of the steel (albeit, the latter cannot be measured). Ningshen et al. [27] observed that for the 316L stainless steel, pre-charging with hydrogen decreased the pitting potential, and increased the passive current density. They claimed that this effect was due to a change in the chemical composition of the passive film due to the presence of diffusible atomic hydrogen. Yuan et al. [30] proposed that the release of atomic hydrogen from the steel (resulting in the ejection of H^+ ions in solution) decreases the local pH, making the passive film more prone to breakdown. Some researchers hypothesised that H could degrade the passive film formed upon steel, by different mechanisms [32, 33, 34, 35], while others claimed that absorbed H promotes a surface-cleaning effect, favouring enhanced anodic dissolution [31].

Overall, the exact reason for the increase in metal dissolution kinetics due to the presence of atomic hydrogen is still not clear, nor is it clear whether electrochemically measured dissolution kinetics actually represent “ionisation”, i.e. metal loss (and not a parallel reaction). A yet unproven possibility includes that atomic hydrogen may oxidise to protons (H^+) by reaction (1), contributing to enhanced currents.

$$H \rightarrow H^+ + e^- \quad (1)$$

With that rationale, assuming a hydrogen concentration in the range 2–18 wppm for an ultra-high strength steel and a diffusion coefficient for H on the order 10^{-9} cm^2/s [43], for a H-containing thickness close to 100 μm the resultant current would be in the range of tens of microamperes. This is a low current, and may be perhaps partially relevant in the context of pitting corrosion of stainless steels, but not greatly significant. Another possibility is iron oxide could be reduced by hydrogen [44], thus destabilising any passive film, thus promoting localised corrosion and resulting in enhanced steel dissolution. It has also been proposed, that at the sub-surface level, the presence of H in the steel lattice could weaken the

http://dx.doi.org/10.1016/j.heliyon.2016.e00209

Fe−Fe bonds (suggested in one study to reduce bond strength ~30%) [45], which correspondingly could lower the activation energy for Fe dissolution; possibly explaining H activated anodic dissolution.

In the present work, to clarify the effect of H-charging upon steel dissolution, for the first time, real-time atomic emission spectroelectrochemistry (AESEC) has been used. This technique, based on the coupling of an electrochemical flow cell with an inductively induced plasma-atomic emission spectrometer (ICP-OES), provides simultaneous information of instantaneous Fe dissolution rates under potentiodynamic polarisation and the corresponding elemental analysis from ICP-OES. Such a technique, can definitively clarify whether it is indeed Fe dissolution, or H-oxidation (1) contributing to the enhanced anodic kinetics recorded from H charged steel samples. These tests were conducted in a non-passivating (acidic) electrolyte, to isolate the effect of H on steel dissolution from its well-known effects on passivity/passivity-breakdown [26, 27, 28, 29, 30, 31, 32, 33, 34, 35]. First principles modelling, on the effect of interstitial H on the local Fe−Fe metallic bonding was also carried out, to estimate the extent of H-driven decohesion, for its discussion with respect to Fe dissolution.

2. Materials

The steel used in this study was AISI 1018 low carbon steel with a nominal carbon content of <0.2%. This steel also has Mn < 0.9%, P < 0.04% and S < 0.05%. The effective hydrogen diffusivity in this low carbon steel is estimated to be close to 10^{-7} cm^2/s [46]. Specimens were 1 mm thick and prepared to a 2000 grit (SiC) finish from rolled AISI 1018 sheet, after which they were rinsed with deionised water, dried with a jet of compressed air, and then finally cleaned with ethanol. The dimensions of the sheet were 50 × 20 mm.

3. Methods

3.1. Electrochemical hydrogen pre-charging

Electrochemical hydrogen pre-charging was carried out for an electrolyte exposed area of 4 cm^2, with the steel subject to cathodic polarisation at −1.632 V_{SCE} (corresponding to a hydrogen overpotential, η_H, of −800 mV) for 24 hours in quiescent 0.6 M NaCl adjusted with NaOH to pH 10. In this study, a high cathodic overpotential was used to introduce H into the steel sample, and similarly an aggressive non-passivating environment (pH 1.95) was used to study the corrosion and dissolution of the H-charged steel. These conditions do not replicate/simulate any specific service condition experienced by this steel, but are used to study the effect of H on Fe dissolution, in the absence of a passive film upon the Fe surface. Following hydrogen pre-charging, samples were immediately transferred to the AESEC flow cell. The diffusible hydrogen concentration within the steel samples,

http://dx.doi.org/10.1016/j.heliyon.2016.e00209

after cathodic charging, was estimated using the so-called barnacle cell method [47].

3.2. The barnacle cell method for determining the absorbed diffusible hydrogen concentration ($C_{H,diff}$)

H extraction (oxidation) was performed in a barnacle cell, wherein, the H-charged samples were polarised at +330 mV vs (SCE) in de-aerated 0.1 M NaOH, to oxidise the diffusible absorbed hydrogen ($C_{H,diff}$). De-aeration was achieved by purging the electrolyte with N_2 gas for 60 minutes prior to polarisation, and this condition was also maintained during the H extraction tests.

3.3. AESEC analysis

The open circuit dissolution rates and potentiodynamic polarisation curves of the uncharged and H-charged samples were measured in 0.6 M NaCl + 0.05 M HCl, at pH 1.95. This solution was prepared from analytical grade salt (VWR International, France) and HCl 30% (Merck, France) diluted with MilliQ water (Millipore, France, 18 MΩ.cm, TOC 3ppb). Atomic emission spectroelectrochemistry (AESEC) was also performed, allowing downstream analysis of dissolution using on-line ICP coupled with electrochemical control. The cell schematic of the AESEC technique is shown elsewhere [48, 49], and the instrumentation required for AESEC includes: an electrochemical flow cell where a flat solid material is exposed to a flowing electrolyte; a downstream ICP-OES spectrometer that is used to analyse the elemental composition of the electrolyte leaving the flow cell; and a special electronic system that is used to collect the emission intensities and electrochemical data as a function of time.

A commercial inductively coupled plasma atomic emission spectrometer was used in this work (HORIBA Jobin Yvon Ultima 2C^{TM}). This consists of a 40.68 MHz inductively coupled Ar plasma, operating at 1 kW, interfaced to independent poly- and mono-chromator optical modules [49]. The ICP-OES calibration was performed using blank solution and matrix-matched Fe standard solutions in a concentration range from 1 to 50 mg/l. Typical limits of detection, calculated as two times the standard deviation of the blank solution measured for at least 5 min, are the following: 0.0061 ± 0.0013 ppm for Fe and 0.0022 ± 0.0006 ppm for Mn. Only concentrations above the detection limits were taken into account.

A Gamry Reference 600 potentiostat was used for all electrochemical experiments. The signals were specially adapted so that they could be channelled into the ICP-OES spectrometer and collected simultaneously with the ICP-OES software [49, 50]. The conditions of electrochemical testing for AESEC included the use of a quiescent electrolyte of 0.6 M NaCl + HCl 0.05 M (pH = 1.95). This slightly acidified electrolyte was chosen in order to ensure that any dissolved Fe remained

http://dx.doi.org/10.1016/j.heliyon.2016.e00209

soluble and hence allowed complete detection in the ICP-OES spectrometer downstream, as at this pH, Fe remains a dissolved species and no stable product can form upon steel, enabling one to independently study the influence of H on Fe dissolution. The exposed electrode area was 0.50 cm^2, with an electrolyte flow rate of 1.20 ml/min. Specimens were exposed for 2 min at open circuit (OCP), and potentiodynamic polarisation was executed from −20 mV below OCP to −100 mV vs. SCE at a scan rate of 1 mV/s. H-precharging was completed just prior to AESEC, and specimens were immediately transferred to the flow cell. The duration at OCP was selected to be 2 mins to minimise the time available for H to diffuse out of the pre-charged specimens. Further, the acidic test electrolyte also allowed for rapid OCP stabilisation and charging of the electrochemical double layer.

3.4. First principles modelling on the effect of interstitial H on Fe−Fe bonding

To understand the effect of absorbed hydrogen on the interatomic bond structure of bcc Fe, we performed calculations using the spin-polarized density functional theory (DFT), with the Generalised Gradient Approximation-Perdew Burke Ernzerhof (GGA-PBE) approximation, as implemented using the Vienna ab-initio simulation package (VASP) [51, 52]. The electronic structure of the bulk bcc Fe was calculated using a kinetic energy cut-off of 500 eV and a Monkhorst-Pack scheme with a 21 × 7 × 3 k-point mesh. The optimised crystal structure was achieved by allowing the lattice cell vectors and ionic positions to relax until the Hellmann-Feynman forces were less than 0.01 eV/Å. The optimised lattice parameter of Fe was obtained to be 2.83 Å, which is consistent with the experimental value [53]. The same calculation parameters were used for a 1 × 3 × 7 bcc Fe supercell with a single H interstitial, positioned separately at the octahedral and tetrahedral site. The electronic bonding charge densities were firstly calculated using VASP and then the 2D contour plots of the electronic charge densities along the (110) and (001) planes of the Fe lattice were generated using VESTA [54]. The Bader atomic volumes were computed by the algorithm developed by Henkelman et al. [55] using the total electronic charge density. The spin and valence electron densities were then integrated over the Bader volumes to estimate the net charges on each atom [56, 57] within the Fe supercell.

4. Results and discussion

4.1. Determination of the absorbed diffusible hydrogen concentration ($C_{H,diff}$)

$C_{H,diff}$ corresponds to the resident mobile H atoms within the steel lattice. In fact, it is the diffusible H atoms that constantly replenish the surface, as H atoms exit the

http://dx.doi.org/10.1016/j.heliyon.2016.e00209

metal at the exit faces. $C_{H,diff}$ is therefore is one of the appropriate parameters to define the H atoms which could impact the electrochemical characteristics of the steel.

The profile of i vs. t, with i corresponding to H oxidation in the barnacle cell is shown in Fig. 1.

These oxidation currents have been corrected for background H-oxidation currents, which were obtained by performing similar measurements upon uncharged samples. This background H oxidation current data has also been presented in Fig. 1. The inset plot shows the relation between log i and log t, with the slope of the plotted data tending towards −1/2. This indicates that the H oxidation current is diffusion controlled, and the following relation (2) holds in this regime.

$$C_{H,diff} = \frac{i_t}{zF}\left(\frac{D_{H,eff}}{\pi t}\right)^{-\frac{1}{2}} \tag{2}$$

Where, i_t is the current at a certain time. z is 1, and $D_{H,eff}$ is taken as 10^{-7} cm^2/s [46]. The above relation could thus be used to derive $C_{H,diff}$ at a particular time. Here, the time at which $C_{H,diff}$ is computed is 600 s (indicated). The average value of $C_{H,diff}$ from the above three measurements was found to be 0.72 ppmw.

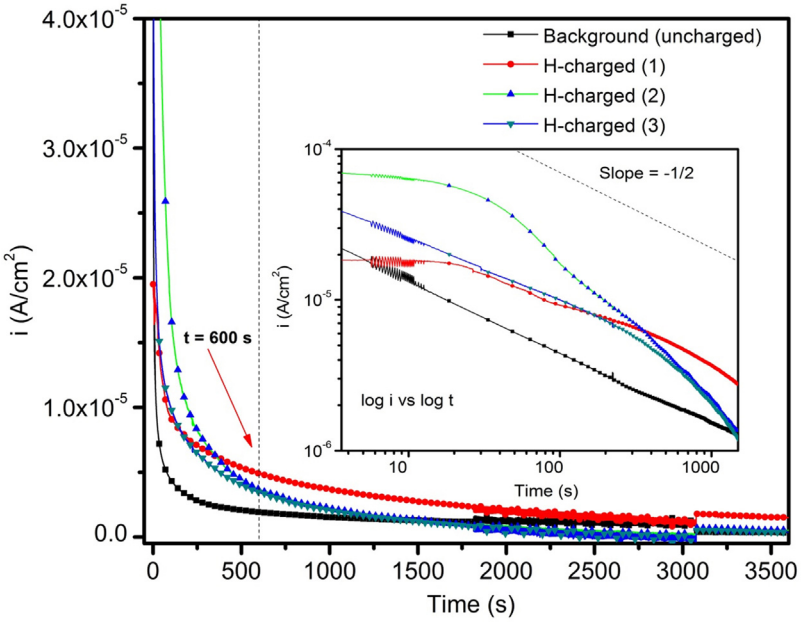

Fig. 1. The H extraction/oxidation currents (i) from three H-charged samples, and also an uncharged (background) sample, plotted as a function of time. The H extraction was performed in 0.1 M NaOH (with pH 12.75), under de-aerated conditions, using a barnacle cell set-up [43, 47]. The inset plot shows that log i vs log t, has a slope close to −1/2. The H oxidation current at t = 600 s, is used to estimate $C_{H,diff}$ associated with the controlled cathodic charging using (2).

http://dx.doi.org/10.1016/j.heliyon.2016.e00209

4.2. The effect of hydrogen on electrode potential and open circuit dissolution of steel

Hydrogen pre-charged steel presents a lower corrosion potential (E_{corr}) when compared to uncharged 1018 steel, as seen in Fig. 2. The concentration of dissolved Fe ions [Fe] ejected into the downstream electrolyte during open circuit dissolution as measured by the ICP is also shown in Fig. 2. The other alloying elements (importantly Mn) in the downstream electrolyte were also measured. The ratio of the Mn to Fe concentration in the downstream electrolyte was observed to be constant for the uncharged sample and the H charged sample prior to potentiodynamic polarisation, implying that the effect of cathodic charging on the surface alloy composition of this steel is negligible (Refer Fig. 3, Fig. 4).

The [Fe] from the hydrogen pre-charged steel is significantly higher than that released from the uncharged steel sample (Fig. 2). This is the first time where it has been shown by an on-line measurement that more Fe dissolves when hydrogen is

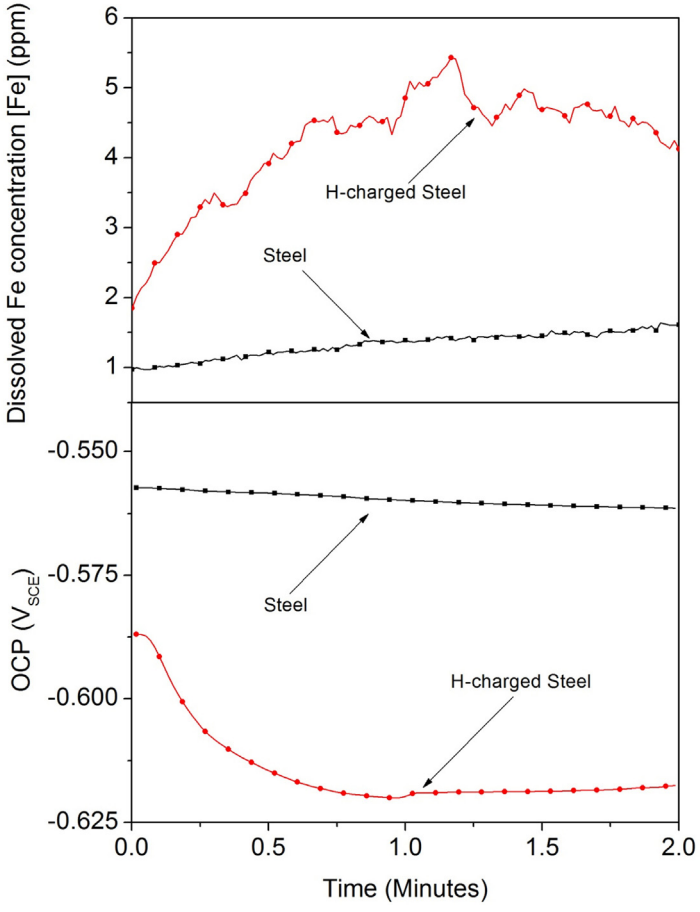

Fig. 2. (Top) The dissolved Fe concentration [Fe] (in ppm), determined by AESEC, (Bottom) The open circuit potentials (OCP) of H-charged steel and uncharged steel, when exposed to 0.6 M NaCl at pH 1.95.

http://dx.doi.org/10.1016/j.heliyon.2016.e00209

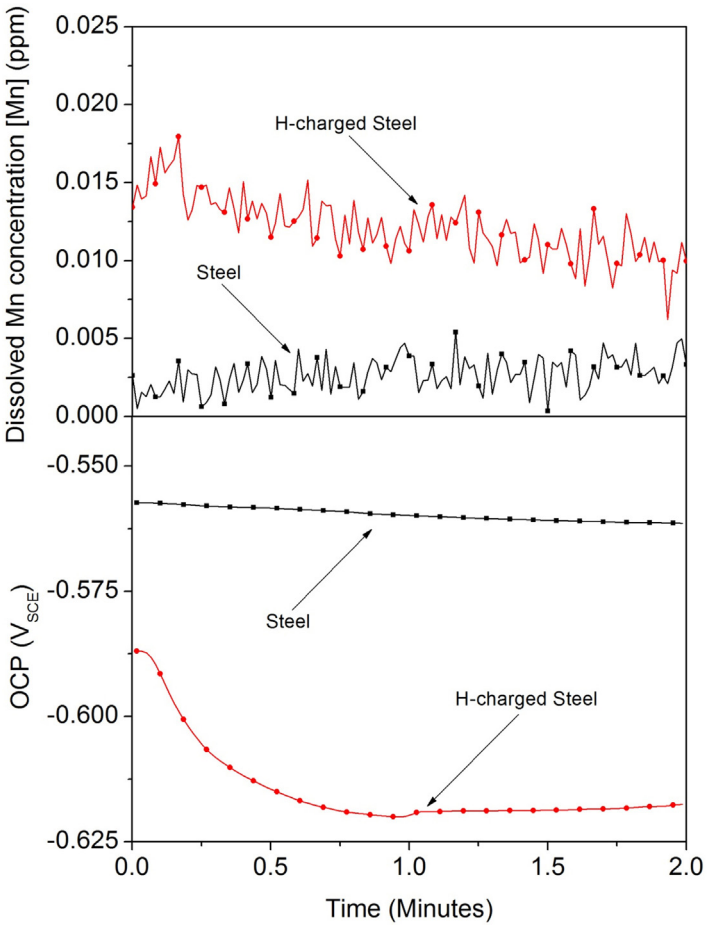

Fig. 3. (Top) The dissolved Mn concentration [Mn] (in ppm), from the uncharged and H-charged 1018 steel samples, at OCP (during free corrosion), and prior to potentiodynamic polarisation, as determined by AESEC. (Bottom) The corresponding OCPs in 0.6 M NaCl at pH 1.95.

present in the steel lattice. The [Fe] released from the H pre-charged sample is greater than that of the uncharged samples by ~200 to 500%. The enhanced Fe dissolution (increased metal dissolution kinetics) is concomitant with the E_{corr} of steel being less noble.

4.3. The enhanced dissolution of H charged steels during anodic polarisation

The [Fe] values detected in the downstream electrolyte during potentiodynamic polarisation of both the H-charged and uncharged steels are shown in Fig. 5. The dissolution rate of the H-charged steel (i_{corr}: 0.68 mA/cm^2) is significant, and appreciably higher than that of the uncharged steel (i_{corr}: 0.23 mA/cm^2). The potentiodynamic polarisation curves of both the uncharged and H-charged samples are shown in Fig. 6, along with the corresponding calculated current equivalents as derived from the [Fe] values, detected by ICP-OES.

http://dx.doi.org/10.1016/j.heliyon.2016.e00209

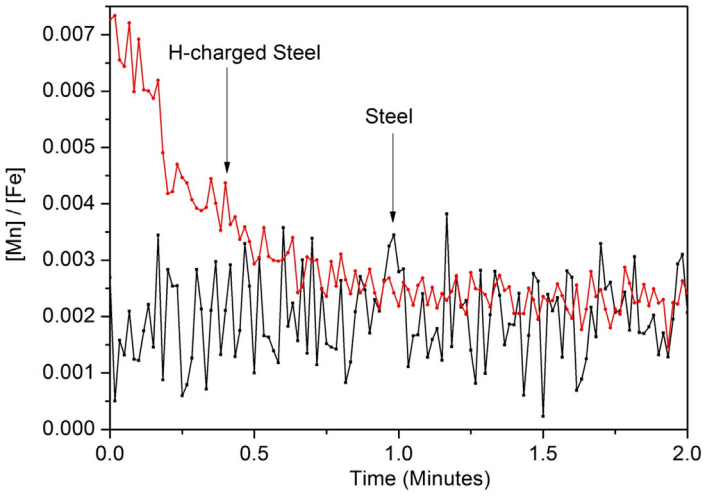

Fig. 4. The ratio of dissolved Mn concentration [Mn] to dissolved Fe concentration [Fe], plotted as a function of time, for both the uncharged and H-charged 1018 steel samples, during free corrosion. The samples were both exposed to 0.6 M NaCl at pH 1.95. The data corresponding to [Mn], can be inferred from Fig. 3, whereas the data corresponding to [Fe] could be inferred from Fig. 2 (in the manuscript). The [Mn]/[Fe] ratio for both the samples, are nearly constant after about 1 minute exposure, implying that the effect of cathodic charging upon Mn, and other elements in 1018 steel is negligible.

It can be seen that the kinetics of the anodic dissolution are more rapid for the H-charged specimen, and also that the [Fe] released from the H-charged steel sample is higher than that released from the uncharged sample. The profile of the potentiodynamic polarisation curve and the anodic current densities reveal that the

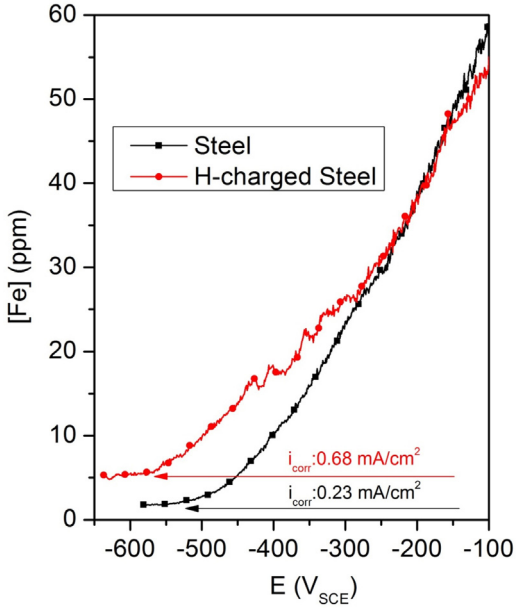

Fig. 5. [Fe] (in ppm) in the downstream electrolyte during potentiodynamic polarisation of the H-charged and uncharged 1018 steel samples in 0.6 M NaCl (at pH 1.95), as detected by ICP-OES.

http://dx.doi.org/10.1016/j.heliyon.2016.e00209

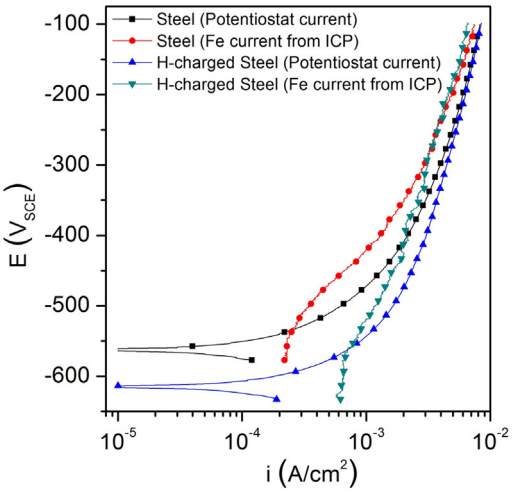

Fig. 6. Potentiodynamic polarisation and overlaid AESEC determined current densities (from dissolved Fe-ions) as a function of applied potential for H-charged and uncharged 1018 steel samples in 0.6 M NaCl (pH 1.95).

1018 steel studied is not passive under the testing conditions herein. The polarisation curves of both the H-charged and the uncharged samples tend towards each other from about −0.3 V_{SCE}, which corresponds to high current densities.

The current densities as deduced from the ICP-OES measurement of Fe ions (i_{ICP}) are compared with that recorded by the potentiostat ($i_{potentiostat}$) in Fig. 7. For relatively low anodic current densities (< 2000 μA/cm^2) i_{ICP} is greater than $i_{potentiostat}$, indicating that more Fe dissolves than that corresponding to the charge supplied by the potentiostat. This may be expected on the basis that the free corrosion rate (at open circuit) is in itself appreciable and the application of small potentials results in only weak polarisation, where the net anodic current is less than the true anodic current density. It may also imply that that there is an activation of Fe dissolution, in the H-charged samples. We note however, that the anodic current densities measured at E_{corr}, are obviously well in excess of > 100 μA/cm^2, whilst the currents (i) arising from hydrogen oxidation (1) would have been < 100 μA/cm^2 if estimated from (3), when $C_{H,diff}$ (the diffusible hydrogen concentration) is taken to be in the range up to 1 wppm.

$$i = \frac{n \cdot F \cdot D_{H,eff} \cdot C_{H,diff}}{L} \tag{3}$$

Where, n is the number of electrons transferred during the electrochemical reaction, F is the Faraday's constant (96485C/mole), L is assumed as 100 μm and $D_{H,eff}$ is the effective diffusion coefficient (10^{-7} cm^2/s). $C_{H,diff}$ has the unit mol/cm^3. The estimation from (3) indicates that the current contribution from reaction (1) is significantly lower than that corresponding to Fe dissolution. This implies that the relatively higher anodic currents from H-charged samples, are mainly due

http://dx.doi.org/10.1016/j.heliyon.2016.e00209

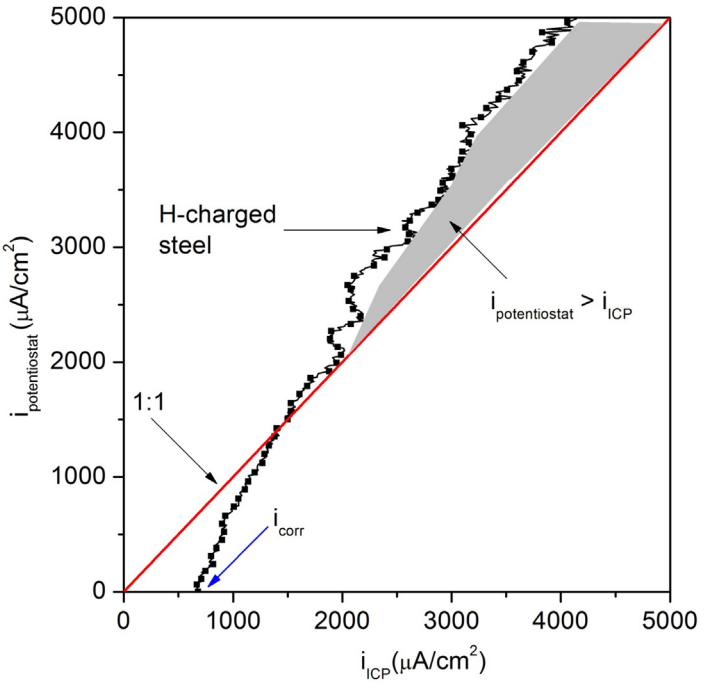

Fig. 7. The anodic current measured by the potentiostat during potentiodynamic polarisation, $i_{potentiostat}$, plotted against the corresponding current as determined from ICP-OES measurements, i_{ICP} (from dissolved Fe ions), for the H-charged 1018 steel.

to enhanced dissolution of Fe ions rather than H oxidation or associated processes. At higher anodic current densities, $i_{Potentiostat}$ is greater than i_{ICP} indicating that some of the dissolved Fe ions may form some insoluble corrosion products on the surface.

H can exist in five possible states, within such a metal-electrolyte system; H_2, H_3O^+, H_{ads}, and also H_{abs} (octahedral), H_{abs} (tetrahedral) and H_{abs} (traps). The equilibrium electrode potential (in V_{SCE}) for the H^+/H_2 reaction (4), is given by (5), whereas the equilibrium electrode potential (in V_{SCE}) for the H^+/H reaction (6), is given by (7) [58].

$$H_2 \leftrightarrow 2H^+ + 2e^- \tag{4}$$

$$E_{H^+/H_2} = -0.244 - 0.0591\,pH - 0.00295\log \rho_{H_2} \tag{5}$$

$$H \leftrightarrow H^+ + e^- \tag{6}$$

$$E_{H^+/H} = -0.244 - 2.106 - 0.0591\,pH - 0.00295\log\rho_H \tag{7}$$

At pH 1.95 neglecting the partial pressure (ρ) terms of (4) and (5), E_{H^+/H_2} is −0.359 V_{SCE} and $E_{H^+/H}$ is −2.46 V_{SCE}. The E_{corr} of the H-charged steel is around −0.6 V_{SCE}, and in this potential range, (4) is more feasible in the cathodic direction, thus favouring the recombination of H to form H_2, while (6)

http://dx.doi.org/10.1016/j.heliyon.2016.e00209

is 'anodic', favouring H oxidation. The atomic hydrogen absorbed in the steel, near −0.6 V_{SCE}, could therefore both undergo recombination to form H_2, or undergo oxidation at the same time as protons in the acid are reduced, and this is thermodynamically acceptable. At potentials anodic to −0.359 V_{SCE}, reaction (4) is favoured in the anodic direction, resulting in a large concentration of H atoms being oxidised to H^+ at the metal-solution interface. Conceivably, once most of the absorbed hydrogen has been oxidised, at potentials >> −0.359 V_{SCE} the H-charged sample and the uncharged sample show a similar electrochemical behaviour (Fig. 6). It must be noted that the charging conditions adopted herein are very severe to demonstrate the impact of absorbed H on metal dissolution. It remains to be determined how much effect there will be of absorbed H on metal dissolution, in more "field-like" or practically relevant charging conditions while allowing for crack-tip localisation. This aspect will be explored in the future work.

4.4. The effect of interstitial H on the metallic bonding in Fe

H has a low solubility in Fe. The H solubility in pure Fe at ambient temperature is in the range 0.0001 to 0.001 ppm [59]. The heat of solution at infinite dilution is 20 eV per H atom [60]. It therefore either diffuses through the Fe lattice or is trapped at defects within the Fe lattice. Interstitial lattice diffusion is therefore a prominent mode of H transport through the steel. The effects of interstitial hydrogen within the Fe lattice (along the 100 and 110 planes) on the electronic bonding charge densities are shown in Fig. 8. The H atom was positioned both at the tetrahedral and octahedral interstitial sites for the DFT calculations. From Fig. 8 it can be inferred that the electron density in the vicinity of the interstitial H atoms is much higher relative to H-free interstitial positions. It can also be seen that the presence of H, decreases the electron density close to the neighbouring Fe atoms. The increase in electron density between Fe and H, occurs at the expense of a decrease in electron density between the neighbouring Fe atoms, resulting in the weakening of the local Fe−Fe bonds. The charge on each atom was estimated from the total electron density using the Bader analysis. The normalised Fe charge is defined as the difference between the charge on each Fe atom in the presence of the H interstitial and the same Fe atom in the absence of the H interstitial. Fig. 9 and Fig. 10 reveal the normalised Fe charge along the (010) plane in the presence of octahedral and tetrahedral H respectively plotted versus the distance between the H interstitial and the Fe atom.

The calculations revealed that a transfer of 0.17 e^- takes place from the 1st nearest neighbouring (NN) Fe atom to the H atom at an octahedral interstitial site. Similarly, in the presence of a tetrahedral H interstitial, a transfer of 0.25 e^- takes place from the 1st nearest neighbouring (NN) Fe atom to the H interstitial. This electron transfer moderately impacts the electron density of the 2nd NN Fe atom,

http://dx.doi.org/10.1016/j.heliyon.2016.e00209

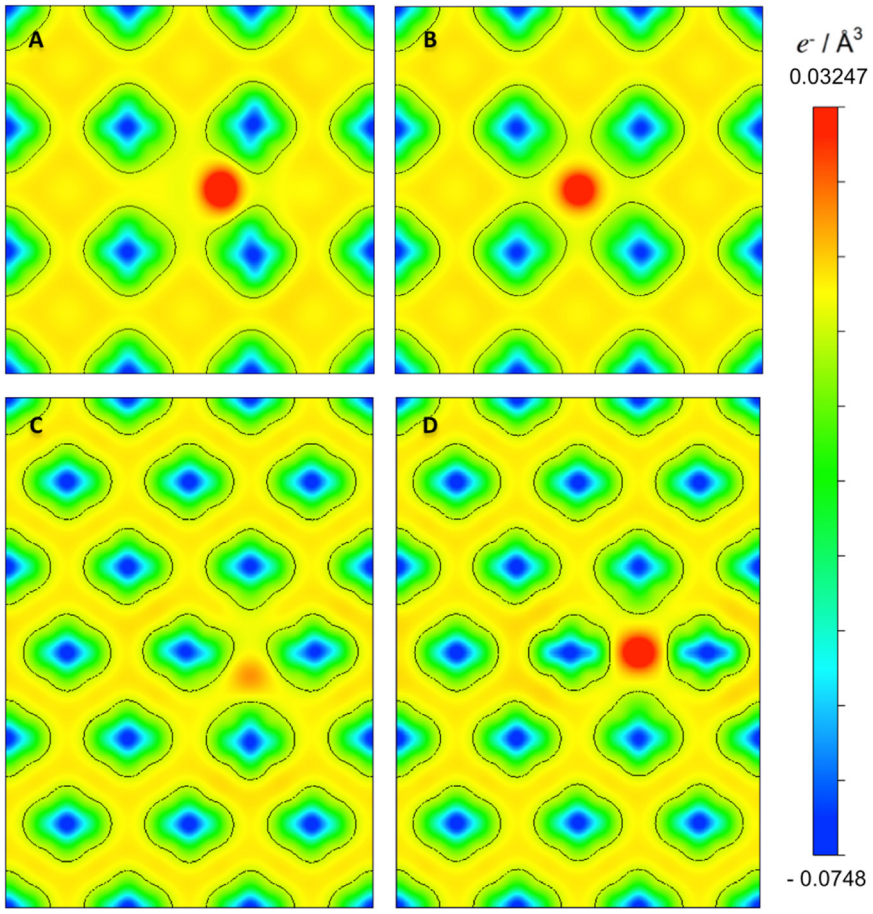

Fig. 8. The distribution of electronic bonding charge densities (e^{-}/Å^{3}) in bcc Fe (Fe sites shown in blue) with H interstitial (in red) on (001) sections at (A) tetrahedral site and (B) octahedral site, and on (110) sections at (C) tetrahedral site and (D) octahedral site.

however, the impact is minimal further away from the 2nd NN. The Bader charge analysis also revealed that H atom at the tetrahedral and octahedral interstitial site respectively were negatively charged by 0.56 e^{-} and 0.52 e^{-} respectively.

Overall, the octahedral H interstitial has six 1st NN, and thirty-four 2nd NN, whereas, the tetrahedral H interstitial has eight 1st NN, and thirty 2nd NN. The presence of a single H interstitial can therefore influence the bonding of at least 40 Fe atoms (octahedral H interstitial), and at least 38 Fe atoms (tetrahedral H interstitial), overall resulting in the weakening of the Fe bond strength. The weakening of Fe−Fe bonds due to the presence of interstitial H within the Fe lattice has been shown in several similar models in the literature [45, 60, 61, 62, 63, 64, 65, 66]. When H is present at an interstitial position within the Fe lattice an electron transfer of around 0.35 e^{-} to 0.6 e^{-} takes place from the Fe atom to the neighbouring H atom [45, 60, 66], which is well in the range of our estimation. The weakening of the Fe−Fe bond due to the presence of H in the Fe lattice, is

http://dx.doi.org/10.1016/j.heliyon.2016.e00209

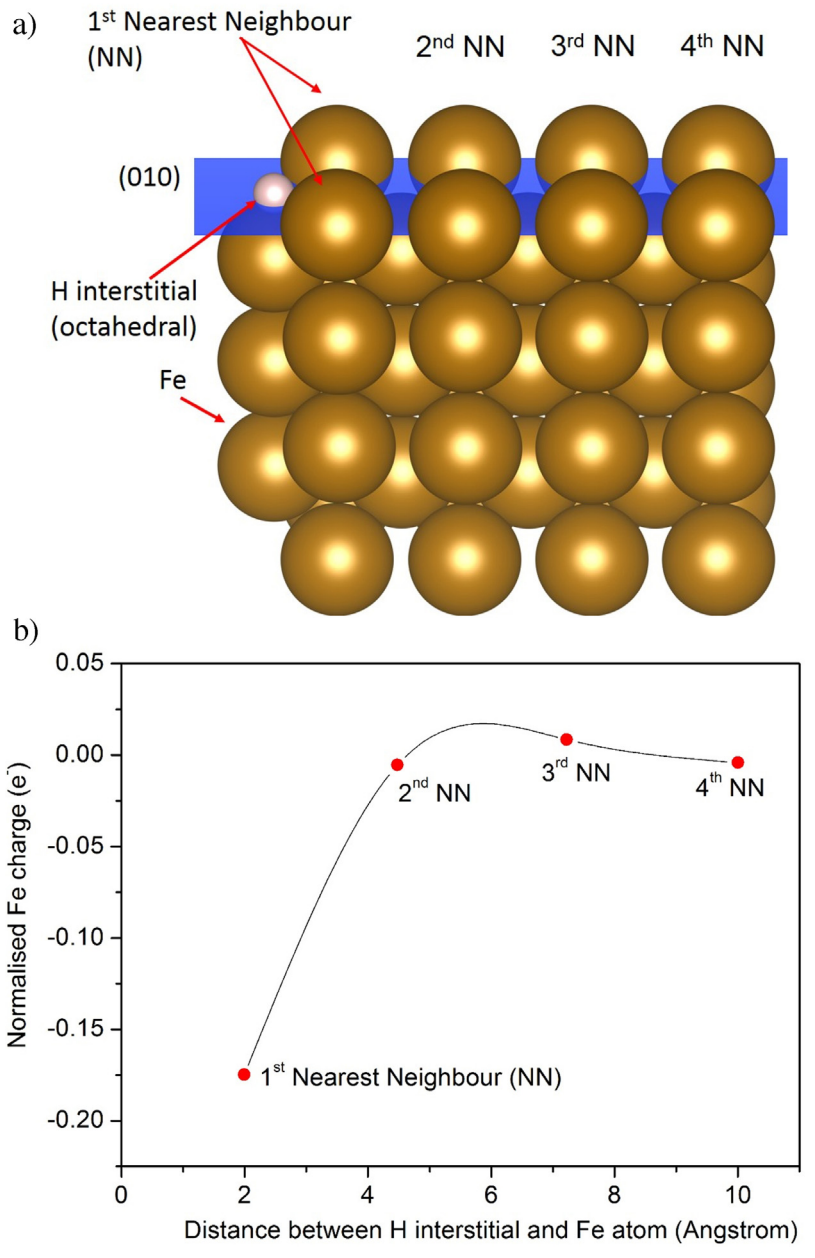

Fig. 9. a) The (010) plane cross-section of BCC Fe with an octahedral H interstitial; b) The normalised Fe charge distribution impacted by the presence of the octahedral H interstitial, as calculated by the Bader charge analysis.

estimated to be close to 30%, by both Saravia et al. [65] and Juan et al. [45]. At the Fe-solution interface, this translates to a decrease in the activation energy for Fe atoms to dissolve into Fe^{2+} ions, by about 30%, in H containing areas. However, the actual enhancement of Fe dissolution in H-charged steels (Fig. 2, Fig. 5, Fig. 6), was found to be significantly higher (range: 200–500%), than that estimated by considering just Fe−Fe bond weakening (range: 30–35%). Moreover,

http://dx.doi.org/10.1016/j.heliyon.2016.e00209

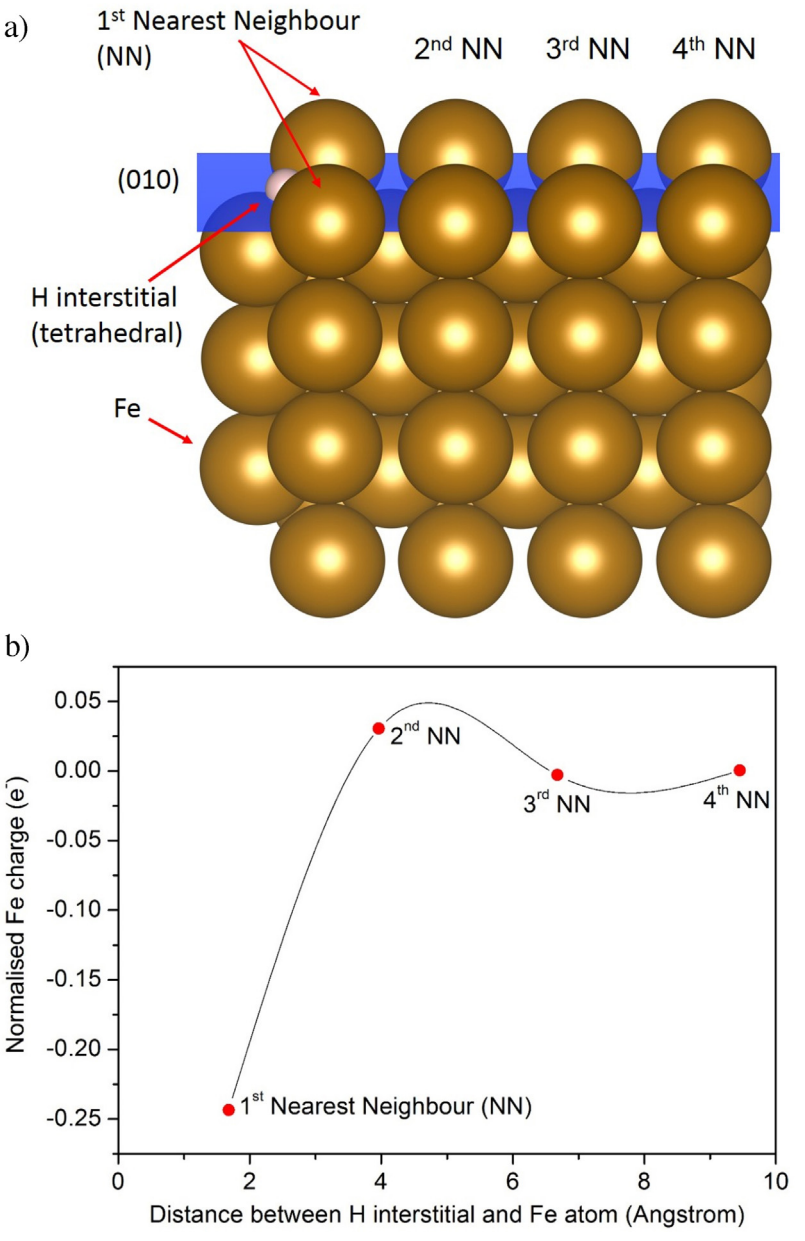

Fig. 10. a) The (010) plane cross-section of bcc Fe with the tetrahedral H interstitial; b) The normalised Fe charge distribution impacted by the presence of the tetrahedral H interstitial, as calculated by the Bader charge analysis.

it must be noted that only 1 ppmw of diffusible H is present in the steel, which affects nearest neighbouring Fe−Fe bonds, and not bulk Fe metallic bonding. The enhanced Fe dissolution of H charged samples, therefore, cannot be readily explained by H-driven Fe−Fe bond weakening alone.

It is interesting to note that the ab-initio calculations indicate that H is negatively charged, when located at the interstitial sites with the Fe lattice (Fig. 8, Fig. 9,

http://dx.doi.org/10.1016/j.heliyon.2016.e00209

Fig. 10). Since H has a low solubility in the Fe lattice it tends to readily diffuse through steel and exit the metal depending the on concentration/pressure gradients. When the H-charged steel is exposed to ambient atmosphere, H could exit the metal in the form of a gas. However, when the steel is in contact with an aqueous solution (as in current scenario) H could either get oxidised by (6) to form H^+, undergo recombination (4) or directly reduce oxygen [25]. The equilibrium electrode potential of the H/H^+ reaction is around -2.46 V_{SCE} and is less noble than the equilibrium electrode potential of the Fe/Fe^+ reaction (around -0.68 V_{SCE}) [58]. The H-charged steel therefore settles at a less noble OCP than the uncharged steel (Refer Fig. 2) and H oxidation to H^+ is more favoured at the metal surface.

4.5. General discussion

During cathodic charging of steel, the hydrogen evolution reaction (4) taking place upon the steel surface, usually involves a step where H atoms are adsorbed onto the metal surface forming $MH_{(ads)}$. The Volmer-Tafel mechanism for hydrogen evolution [67] is presented below (8)–(9).

$$M + H_3O^+ + e^- \rightarrow MH_{(ads)} + H_2O \quad (8)$$

$$MH_{(ads)} + MH_{(ads)} \rightarrow 2\ M + H_2 \quad (9)$$

The adsorbed hydrogen atoms may be absorbed into the steel lattice (10) forming $MH_{(abs)}$, and in the case of steel, a Fe−H bonds develop between the interstitial H atoms and the neighbouring Fe atoms.

$$MH_{(ads)} \leftrightarrow MH_{(abs)} \quad (10)$$

The formation of this Fe−H bond, is manifested by the increase in electron density between Fe and H, and a corresponding decrease in electron density between neighbouring Fe atoms (Fig. 8). H atoms diffuse through the Fe lattice during cathodic charging surrounded by clouds of conducting electrons [62].

When the cathodic charging (i.e. H-charging) is ceased, and the H-charged samples are at OCP, H has an intrinsic tendency to exit steel. This is because H has a low solubility in Fe [59, 60], and also being a strong reducing agent [24], it immediately reduces the contacting species, like oxygen [25], or the iron oxide film [44, 68] (and where relevant, even Fe^{3+} to Fe^{2+}). H could also react with oxygen to form the peroxyl species ($HO_2^{\cdot}$), which could further oxidise Fe^{2+} to Fe^{3+} and also contribute towards other parallel reactions; this effect however has not been investigated yet. H atoms may also undergo chemical recombination to form H_2. As H exits the steel, the Fe−H bonds formed during cathodic charging are disrupted, and the Fe atoms previously bonded to H, after the Fe−H bond disruption become active sites for chemical/electrochemical reactions. The

http://dx.doi.org/10.1016/j.heliyon.2016.e00209

impedance response of passive iron electrodes during/after hydrogen permeation, in borate buffer solutions, revealed the presence of an inductive component at low frequencies [44]. The inductive behaviour further validates that H absorption steel, makes the iron surface active, or activates the intermediate [44], and implies that there is acceleration/activation of the anodic reaction [69]. The exact reason for H driven anodic dissolution is still not completely clarified, the weakening of Fe−Fe bonds due to the presence of interstitial H is one factor, and however this alone cannot explain a 200–500% increase in anodic current densities arising from H charged steel samples on the basis of concentrations at ~ 1 ppm. However, in this context, it must be noted that, firstly, the surface/sub-surface hydrogen concentration is significantly higher than the bulk hydrogen concentration (1 ppmw). The first few monolayers of the metal surface, serve as a high energy trap sites for hydrogen, and thus may contain a higher concentration of interstitial H, than the bulk metal [70]. Ab-initio calculations have shown that the ideal fracture energy of the Fe decreases linearly with H coverage [71]. In fact, for Fe it was found that the ideal fracture energy decreases by about 45%, when the surface is covered by one half monolayer of H atoms [71]. The presence of hydrogen in the metals (especially at the surface/sub-surface) could stabilise free vacancies in bcc Fe in the form of solute-vacancy clusters [72], and also could result in the formation of super-abundant vacancies in the metal [73]. The impact of such processes on the electrochemistry/corrosion of metals are not well studied and will need to be explored in future research on this topic.

The current environmentally assisted cracking (EAC) models for hydrogen embrittlement [74], do not incorporate, nor account for, the local chemical/electrochemical effects arising from the presence/exit of absorbed H. H, besides activating the anodic dissolution (this work), and promoting pit initiation/propagation [26, 27, 28, 29, 30, 31, 32, 33, 34], could also reduce a number of species in the electrolyte [24, 25]; with all these factors causing changes in local chemistry, and consequently impacting EAC. The threshold H concentration below which there is no significant effect of H on steel dissolution, is an important parameter which will need to be determined in future work. This is a complicated parameter to determine, as it depends on the metal/alloy, the cathodic charging current density, and the time elapsed between the cathodic charging and subsequent corrosion testing, etc. H could also directly react with oxygen, and/or the passive film, which could correspondingly influence metal dissolution rates – with a wider study required to tackle this question. In stainless steels, the presence of H promotes pit initiation and pit propagation [26, 27]. As the pit growth is more conducive in the presence of H, correspondingly the pitting to cracking transition will be much faster, than for an uncharged steel sample. H may therefore influence the time for the onset of cracking, by affecting pit initiation/pit propagation. The electrochemical/chemical effects of H on pitting to cracking

http://dx.doi.org/10.1016/j.heliyon.2016.e00209

transition will therefore need to be considered in future modelling efforts. In H_2S environments, the chemical recombination of adsorbed H to H_2 is poisoned upon the steel surface [14, 15], resulting in a higher concentration of absorbed H within such steels, as evidenced by higher recorded H permeation current densities [14, 15]. In such systems, crack growth may be driven by the anodic dissolution arising from the presence of absorbed H.

5. Conclusions

The presence of diffusible atomic hydrogen (at about 1 ppmw) in steel results in increased anodic dissolution by about 200–500%. This was readily evidenced by an increase in anodic currents during potentiodynamic polarisation, and also unambiguously validated via the use of online ICP-OES. It was observed that the H-charged sample, in a non-passivating electrolyte, released an appreciably higher concentration of Fe ions into the electrolyte, when compared to an uncharged sample. This clarifies that H actually intrinsically increases the active dissolution rate of Fe. This finding is thus independent (but related) to the widely reported effect of absorbed H, in increasing the passive current density, pit initiation and pit propagation rate of steels in passivating solutions. The weakening of Fe−Fe bonding due to presence of 1 ppmw H alone cannot rationalise such a large increase in anodic currents, and therefore the effect of H on activating Fe dissolution is not completely clarified.

The concentrations of Fe ions detected in the downstream electrolyte, when the H-charged steel was polarised at potentials close to its E_{corr} were in the range > than 500 $\mu A/cm^2$. This implies that even if tallied by the potentiostat, that the effect of electrochemical oxidation of H (which would be <100 $\mu A/cm^2$) is less significant when compared to the actual enhanced Fe dissolution rate.

The findings herein, whilst on face value may be considered somewhat elementary, have two major implications. Firstly, they definitively answer the question as to the electrochemical role of absorbed hydrogen, and secondly, they indicate that any logical model for environmentally assisted cracking (hydrogen embrittlement) for some steels must give significant emphasis on the enhanced dissolution as a result of hydrogen. The corrosion component of corrosion assisted mechanical failure should now be considered as a key parameter in metal durability.

Declarations

Author contribution statement

Sebastian Thomas, Polina Volovitch, Guruprasad Sundararajan, Nikhil V. Medhekar, Kevin Ogle, John R. Scully: Analyzed and interpreted the data; Wrote the paper.

http://dx.doi.org/10.1016/j.heliyon.2016.e00209

Noemie Ott, Rebecca F. Schaller, Jodie A. Yuwono, Nick Birbilis: Performed the experiments; Analyzed and interpreted the data; Wrote the paper.

Competing interest statement

The authors declare no conflict of interest.

Funding statement

Nick Birbilis was supported by Ecole Nationale Superieure de Chimie de Paris, Centre National de la Recherche Scientifique (ENSCP-CNRS). Rebecca F. Schaller was supported by the 2014 Australia Endeavour Award Research Fellowship. Rebecca F. Schaller and John R. Scully were supported by the US Air Force Academy (agreement number FA7000-13-2-0020).

Additional information

No additional information is available for this paper.

References

[1] G.B. Rawls, T. Adams, N.L. Newhouse, Hydrogen production and containment, In: R.P. Gangloff, B.P. Somerday (Eds.), Gaseous Hydrogen Embrittlement of Materials in Energy Technologies, vol. 2, Woodhead Publishing Series in Metals and Surface Engineering, 2012, pp. 3–50.

[2] A. Turnbull, A.J. Griffiths, Implications of hydrogen uptake and transport for environment assisted cracking testing and interpretation of results, Br. Corrosion J. 31 (1996) 39–43.

[3] W. Chen, R. Kania, R. Worthingham, G.V. Boven, Transgranular crack growth in the pipeline steels exposed to near-neutral pH soil aqueous solutions: the role of hydrogen, Acta Mater. 57 (2009) 6200–6214.

[4] R.S. Irani, Hydrogen storage: high-pressure gas containment, M. R. S. Bull. 27 (2002) 680–682.

[5] A. Traidia, M. Alfano, G. Lubineau, S. Duval, A. Sherik, An effective finite element model for the prediction of hydrogen induced cracking in steel pipelines, Int. J. Hydrogen Energy 37 (2012) 16214–16230.

[6] Corrosion in Aqueous Solutions, 3rd edition, In: L.L. Shreir, R.A. Jarman, G. T. Burstein (Eds.), Corrosion, 1, Butterworth Heinemann, Oxford, UK, 1994, pp. 55–117.

[7] F.D. Fischer, G. Mori, J. Svoboda, Modelling the influence of trapping on hydrogen permeation in metals, Corrosion Sci. 76 (2013) 382–389.

 http://dx.doi.org/10.1016/j.heliyon.2016.e00209

[8] D.G. Enos, A.J. Williams Jr., G.G. Clemena, J.R. Scully, Impressed-current cathodic protection of steel-reinforced concrete pilings: protection criteria and the threshold for hydrogen embrittlement, Corrosion 54 (1998) 389–402.

[9] F. Zucchi, V. Grassi, C. Monticelli, G. Trabanelli, Hydrogen embrittlement of duplex stainless steel under cathodic protection in acidic artificial sea water in the presence of sulphide ions, Corrosion Sci. 48 (2006) 522–530.

[10] T. Kushida, Hydrogen entry into steel by atmospheric corrosion, ISIJ Int. 43 (2003) 470–474.

[11] E. Akiyama, K. Matsukado, M. Wang, K. Tsuzaki, Evaluation of hydrogen entry into high strength steel under atmospheric corrosion, Corrosion Sci. 52 (2010) 2758–2765.

[12] R.N. Parkins, W.K. Blanchard Jr., B.S. Delanty, Transgranular stress corrosion cracking of high-pressure pipelines in contact with solutions of near neutral pH, Corrosion 50 (1994) 394–408.

[13] H.W. Pickering, R.P. Frankenthal, On the mechanism of localized corrosion of iron and stainless steel, I. Electrochemical studies, J. Electrochem. Soc. 119 (1972) 1297–1304.

[14] R.N. Iyer, H.W. Pickering, A mechanistic analysis of hydrogen entry into metals during cathodic hydrogen charging, Scr. Metallurgica 22 (1988) 911–916.

[15] R.N. Iyer, H.W. Pickering, M. Zamanzadeh, Analysis of hydrogen evolution and entry into metals for the discharge-recombination process, J. Electrochem. Soc. 136 (1989) 2463–2470.

[16] J.P. Hirth, Effects of hydrogen on the properties of iron and steel, Metallurgical Trans. A 11 (1980) 861–890.

[17] W.H. Johnson, On some remarkable changes produced in iron and steel by the action of hydrogen and acids, Proc. R. Soc. Lond. 23 (1875) 168–179.

[18] I.M. Robertson, P. Sofronis, A. Nagao, M.L. Martin, S. Wang, D.W. Gross, K.E. Nygren, Hydrogen embrittlement understood, Metallurgical Mater. Trans. A 46A (2015) 2323–2341.

[19] R.A. Oriani, Whitney Award Lecture—1987: Hydrogen—The Versatile Embrittler, Corrosion 43 (1987) 390–397.

[20] S.P. Lynch, Metallographic and fractographic techniques for characterising and understanding hydrogen-assisted cracking of metals, In: R.P. Gangloff, B.P. Somerday (Eds.), Gaseous Hydrogen Embrittlement of Materials in Energy Technologies, Woodhead Publishing Series in Metals and Surface Engineering, 2012, pp. 273–346.

http://dx.doi.org/10.1016/j.heliyon.2016.e00209

[21] S. Lynch, Hydrogen embrittlement phenomena and mechanisms, Corrosion Rev. 30 (2012) 105–123.

[22] W. Gerberich, In: R.P. Gangloff, B.P. Somerday (Eds.), Gaseous Hydrogen Embrittlement of Materials in Energy Technologies, vol. 1, Woodhead Publishing Limited, Cambridge, U.K, 2012, pp. 209–246.

[23] J. Song, W.A. Curtin, Atomic mechanism and prediction of hydrogen embrittlement in iron, Nat. Mater. 12 (2012) 145–151.

[24] W. Li, T. Cochell, A. Manthiram, Activation of aluminum as an effective reducing agent by pitting corrosion for wet-chemical synthesis, Sci. Rep. 3 (2012) 1229.

[25] R.F. Schaller, S. Thomas, N. Birbilis, J.R. Scully, Spatially resolved mapping of the relative concentration of dissolved hydrogen using the scanning electrochemical microscope, Electrochem. Commun. 51 (2015) 54–58.

[26] L.J. Qiao, J.L. Luo, Hydrogen-facilitated anodic dissolution of austenitic stainless steels, Corrosion 54 (1998) 281–288.

[27] S. Ningshen, U.K. Mudali, G. Amarendar, P. Gopalan, R.K. Dayal, H.S. Khatak, Hydrogen effects on the passive film formation and pitting susceptibility of nitrogen containing type 316L stainless steels, Corrosion Sci. 48 (2006) 1106–1121.

[28] M.C. Li, Y.F. Cheng, Mechanistic investigation of hydrogen-enhanced anodic dissolution of X-70 pipe steel and its implication on near-neutral pH SCC of pipelines, Electrochim. Acta 52 (2007) 8111–8117.

[29] Y.F. Cheng, L. Niu, Mechanism for hydrogen evolution reaction on pipeline steel in near-neutral pH solution, Electrochem. Commun. 9 (2007) 558–562.

[30] Y. Yuan, L. Liang, C. Wang, Y. Zhu, Study of the effects of hydrogen on the pitting processes of X70 carbon steel with SECM, Electrochem. Commun. 12 (2010) 1804–1807.

[31] A. Ejaz, Z. Lu, J. Chen, Q. Xiao, X. Ru, G. Han, T. Shoji, The effects of hydrogen on anodic dissolution and passivation of iron in alkaline solutions, Corrosion Sci. (2015), doi:http://dx.doi.org/10.1016/j.corsci.2015.09.013.

[32] J.G. Yu, J.L. Luo, P.R. Norton, Investigation of hydrogen induced pitting active sites, Electrochim. Acta 47 (2002) 4019–4025.

[33] Y.M. Zeng, J.L. Luo, P.R. Norton, Initiation and propagation of pitting and crevice corrosion of hydrogen-containing passive films on X70 micro-alloyed steel, Electrochim. Acta 49 (2004) 703–714.

[34] S. Pyun, C. Lim, R.A. Oriani, The role of hydrogen in the pitting of passivating films on pure iron, Corrosion Sci. 33 (1992) 437–444.

[35] J. Yao, C. Dong, C. Man, K. Xiao, X. Li, 2015. Corrosion, Corrosion In-Press. http://dx.doi.org/10.5006/1811.

[36] B.T. Lu, L.J. Qiao, J.L. Luo, K.W. Gao, Role of hydrogen in stress corrosion cracking of austenitic stainless steels, Philos. Mag. 91 (2011) 208–228.

[37] S.X. Mao, B. Gu, N.Q. Wu, L. Qiao, The mechanism of hydrogen facilitated anodic dissolution type stress corrosion cracking: theories and experiments, Philos. Mag. 81 (2001) 1813–1831.

[38] J. Cwiek, K. Nikiforov, Hydrogen degradation of high-strength weldable steels in seawater, Mater. Sci. 40 (2004) 831–835.

[39] L. Qiao, X. Mao, W. Chu, The role of hydrogen in stress-corrosion cracking of austenitic stainless steel in hot $MgCl_2$ solution, Metallurgical Mater. Trans. A 26 (1995) 1777–1784.

[40] D. Wallinder, G. Hultquist, B. Tveten, E. Hornlund, Hydrogen in chromium: influence on corrosion potential and anodic dissolution in neutral NaCl solution, Corrosion Sci. 43 (2001) 1267–1281.

[41] M. Uhlemann, B.G. Pound, Diffusivity, solubility, and trapping behaviour of hydrogen in alloys 600, 690tt and 800, Corrosion Sci. 40 (1998) 645–662.

[42] J. Hou, Q.J. Peng, K. Sakaguchi, Y. Takeda, J. Kuniya, T. Shoji, Effect of hydrogen in Inconel Alloy 600 on corrosion in high temperature oxygenated water, Corrosion Sci. 52 (2010) 1098–1101.

[43] R.F. Schaller, J.R. Scully, Measurement of effective hydrogen diffusivity using the Scanning Kelvin Probe, Electrochem. Commun. 40 (2014) 42–44.

[44] S. Modiano, J.A.V. Carreno, C.S. Fugivara, R.M. Torresi, V. Vivier, O.R. Benedetti, A.V. Mattos, Changes on iron electrode surface during hydrogen permeation in borate buffer solution, Electrochim. Acta 53 (2008) 3670–3679.

[45] A. Juan, R. Hoffmann, Hydrogen on the Fe(110) surface and near bulk bcc Fe vacancies—a comparative bonding study, Surf. Sci. 421 (1999) 1–16.

[46] M.I. Luppo, J. Ovejero-Garcia, The influence of microstructure on the trapping and diffusion of hydrogen in a low carbon steel, Corrosion Sci. 32 (1991) 1125–1136.

[47] ASTM Standard F1113-87, Standard Method for Electrochemical Measurement of Diffusible Hydrogen in Steels, ASTM, International, West Conshohocken, PA, 2005.

[48] K. Ogle, S. Weber, Anodic dissolution of 304 stainless steel using atomic emission spectroelectrochemistry, J. Electrochem. Soc. 147 (2000) 1770–1780.

[49] K. Ogle, J. Baeyens, J. Swiatowska, P. Volovitch, Atomic emission spectroelectrochemistry applied to dealloying phenomena: I. The formation and dissolution of residual copper films on stainless steel, Electrochim. Acta 54 (2009) 5163–5170.

[50] K. Ogle, Atomic emission spectroelectrochemistry: a new look at the corrosion, dissolution & passivation of complex materials, Corrosion Mater. 37 (2012) 60–67.

[51] G. Kresse, J. Furthmüller, Efficient iterative schemes for ab initio total-energy calculations using a plane-wave basis set, Phys. Rev. B 54 (1996) 11169–11186.

[52] J. Perdew, K. Burke, M. Ernzerhof, Generalized gradient approximation made simple, Phys. Rev. Lett. 77 (1996) 3865–3868.

[53] W. Zhong, G. Overney, D. Tomanek, Structural properties of Fe crystals, Phys. Rev. B 47 (1993) 95–99.

[54] K. Momma, F. Izumi, VESTA: a three-dimensional visualization system for electronic and structural analysis, J. Appl. Crystallogr. 41 (2008) 653–658.

[55] G. Henkelman, A. Arnaldsson, H. Jonsson, A fast and robust algorithm for Bader decomposition of charge density, Comput. Mater. Sci. 36 (2006) 354–360.

[56] R. Bader, Atoms in molecules: a quantum theory, International Series of Monographs on Chemistry, Oxford University Press, 1990.

[57] T.A. Manz, D.S. Sholl, Improved atoms-in-molecule charge partitioning functional for simultaneously reproducing the electrostatic potential and chemical states in periodic and non-periodic materials, J. Chem. Theory Comput. 8 (2012) 2844–2867.

[58] M. Pourbaix, Atlas of Electrochemical Equilibria in Aqueous Solutions, 2nd edition, NACE International, Houston, TX, 1974, pp. 307.

[59] F.G. Wei, K. Tsuzaki, Hydrogen trapping phenomena of martensitic steels, In: R.P. Gangloff, B.P. Somerday (Eds.), Gaseous Hydrogen Embrittlement of Materials in Energy Technologies, vol. 2, Woodhead Publishing Series in Metals and Surface Engineering, 2012, pp. 493–525.

[60] Y. Itsumi, D.E. Ellis, Electronic bonding characteristics of hydrogen in bcc iron: Part I interstitials, J. Mater. Res. 11 (1996) 2206–2213.

[61] M. Puska, R. Nieminen, Theory of hydrogen and helium impurities in metals, Phys. Rev. B 29 (1984) 5382–5397.

 http://dx.doi.org/10.1016/j.heliyon.2016.e00209

[62] S.M. Teus, V.N. Shivanyuk, B.D. Shanina, V.G. Gavriljuk, Effect of hydrogen on electronic structure of fcc iron in relation to hydrogen embrittlement of austenitic steels, Phys. Stat. Sol. A 204 (2007) 4249–4258.

[63] S. Simonetti, D.R. Saravia, G. Brizuela, A. Juan, The effects of a hydrogen pair in the electronic structure of the FCC iron containing a vacancy, Int. J. Hydrogen Energy 35 (2010) 5957–5962.

[64] J. Sanchez, J. Fullea, C. Andrade, P. de Andres, Hydrogen embrittlement of high strength steels, Defect Diffusion Forum 289–292 (2009) 203–209.

[65] D.R. Saravia, A. Juan, G. Brizuela, S. Simonetti, Comparative study of H-atom location, electronic and chemical bonding in ideal and vacancy containing-FCC iron, Int. J. Hydrogen Energy 34 (2009) 8302–8307.

[66] Y. Itsumi, D.E. Ellis, Electronic bonding characteristics of hydrogen in bcc iron: Part II grain boundaries, J. Mater. Res. 11 (1996) 2214–2219.

[67] E.G. Dafft, K. Bohnenkamp, H.J. Engell, Investigations of the hydrogen evolution kinetics and hydrogen absorption by iron electrodes during cathodic polarization, Corrosion Sci. 19 (1979) 591–612.

[68] G. Williams, H.N. McMurray, R.C. Newman, Surface oxide reduction by hydrogen permeation through iron foil detected using a scanning Kelvin probe, Electrochem. Commun. 27 (2013) 144–147.

[69] A.D. King, N. Birbilis, J.R. Scully, Accurate electrochemical measurement of magnesium corrosion rates; a combined impedance, mass-loss and hydrogen collection study, Electrochim. Acta 121 (2014) 394–406.

[70] A. Pundt, R. Kirchheim, Hydrogen in metals: microstructural aspects, Annu. Rev. Mater. Res. 36 (2006) 555–608.

[71] D.E. Jiang, E.A. Carter, First principles assessment of ideal fracture energies of materials with mobile impurities: implications for hydrogen embrittlement of metals, Acta Mater. 52 (2004) 4801–4807.

[72] P.R. Monasterio, T.T. Lau, S. Yip, K.J. Van Vliet, Hydrogen-vacancy interactions in Fe-C alloys, Phys. Rev. Lett. 103 (085501) (2009) 1–4.

[73] Y. Fukai, Formation of superabundant vacancies in M-H alloys and some of its consequences: a review, J. Alloys Compd. 356–357 (2003) 263–269.

[74] R.P. Gangloff, Critical issues in hydrogen assisted cracking of structural alloys, In: S. Shipilov, R.H. Jones, J.-M. Olive, R.B. Rebak (Eds.), Environment Induced Cracking of Metals, Elsevier, Oxford, UK, 2006, pp. 141–166.

 http://dx.doi.org/10.1016/j.heliyon.2016.e00209